On the Dynamics of Flexible Beams Under Large Overall Motions—The Plane Case: Part I

J. C. Simo[1]
Applied Mechanics Division,
Stanford University,
Stanford, CA 94305

L. Vu-Quoc
Structural Engineering and
Structural Mechanics Division,
University of California,
Berkeley, CA 94720

The dynamic response of a flexible beam subject to large overall motions is traditionally formulated relative to a floating frame, sometimes referred to as the shadow beam. *This type of formulation leads to equations of motion of the form* $\ddot{\mathbf{g}}(\dot{\mathbf{y}}, \mathbf{y}, t) = \mathbf{0}$, *that are implicit, nonlinear and highly coupled in the inertia terms. An alternative approach is proposed whereby all quantities are referred to the* inertial *frame. As a result, the inertia term enters linearly in the formulation simply as mass times acceleration. Crucial to this formulation is the use of* finite strain rod theories *capable of treating finite rotations. Numerical examples that involve finite vibrations coupled with large overall motions are presented in Part II of this paper.*

Introduction

The dynamics of a flexible beam undergoing large overall motions is typically formulated relative to a coordinate system that follows the rigid body motion of the beam, sometimes referred to as the shadow beam (Laskin, Likins, and Longman, 1983). The introduction of this floating frame, relative to which the strains in the beam are measured, is motivated by the assumption of infinitesimal strains. This assumption has been used by several authors, such as, to name a few, Ashley (1967), Grotte et al. (1971), de Veubeke (1976), Canavin and Likins (1977), Kumar and Bainum (1980), Kane and Levinson (1981a,b), and Kane et al. (1983). With the assumption of small strains, the use of a floating frame allows a simple expression for the total potential energy of the beam. By contrast, the expression of the kinetic energy of the system takes a rather cumbersome form. The resulting equations of motion, although restricted to small strains, are nonlinear and *highly coupled in the inertia terms* due to the presence of Coriolis and centrifugal effects as well as inertia due to rotation of the shadow beam. Moreover, the Galerkin discretization in space variables, leads to a system of implicit coupled nonlinear differential equations in time of the form $\tilde{\mathbf{g}}(\dot{\mathbf{y}}, \mathbf{y}, t) = 0$ (e.g., Song and Haug, 1980). An essential characteristic of this system is that it cannot be transformed to a standard explicit form $\dot{\mathbf{y}} = \mathbf{g}(\mathbf{y}, t)$, without appending an algebraic constraint.[2]

Thus, use of the mode shapes of the structure as a Galerkin basis, a procedure often employed (see, e.g., Likins, 1974) appears to be of little value in the general case due to the highly coupled nature of the resulting semi-discrete equations. Moreover, the complex nature of these equations has often led to simplifying assumptions; see, e.g., Winfrey (1971), Erdman and Sandor (1972), and Baghat and Willmert (1973). We refer to Song and Haug (1980) for a review of several approaches in the dynamic analysis of mechanisms and machines.

In this paper, we propose an approach based on a philosophy opposite to that outlined above. The kinetic energy of the system is reduced to a quadratic uncoupled form simply by referring the motion of the system to the *inertial frame*. This results in a drastic simplification of the inertia operator, which now becomes *linear and uncoupled*, while the stiffness operator emanating from the potential energy functional becomes nonlinear. Conceptually, the essential step needed in developing this alternative approach is the use of rod theories capable of accounting for large rotations of the beam. It is important to note that the basic characteristic of the appropriate strain measures in these theories—as discussed by Reissner (1972, 1973), Antman (1972, 1974), Simo (1985), and Simo and Vu-Quoc (1985)—is their invariance under superposed rigid body motions.

From a computational standpoint, the substantial advantage of the proposed approach over the traditional shadow beam approach lies in the much simpler structure of the resulting equations. As shown in Part II of this paper, by introducing a Galerkin semi-discretization in the space variables, one obtains the standard nonlinear system of ODE's that typically arises in nonlinear structural dynamics: $\mathbf{M}\,\ddot{\mathbf{q}} + \mathbf{D}\,\dot{\mathbf{q}} + \mathbf{P}(\mathbf{q}) = \mathbf{F}$ (see, e.g., Belytschko and Hughes, 1983). In addition, this approach has the advantage of automatically accounting for large strains. Within the present context, there is little to be gained by introducing at the outset the additional small strain assumption.

As a basis for our discussion, we choose a specific problem

---

[1] Formerly at the University of California, Berkeley.

[2] One can always set $\dot{\mathbf{y}} = \mathbf{z}$, and append the *algebraic constraint* $\mathbf{g}(\mathbf{z}, \mathbf{y}, t) = \mathbf{0}$. This is a DAE system, and not a standard ODE system (Petzold, 1982).

Contributed by the Applied Mechanics Division for presentation at the Winter Annual Meeting, Anaheim, CA, December 7-12, 1986, of the American Society of Mechanical Engineers.

Discussion on this paper should be addressed to the Editorial Department, ASME, United Engineering Center, 345 East 47th Street, New York, N.Y. 10017, and will be accepted until two months after final publication of the paper itself in the JOURNAL OF APPLIED MECHANICS. Manuscript received by ASME Applied Mechanics Division, September 23, 1985; final revision, May 7, 1986. Paper No. 86-WA/APM-41.

$$\begin{Bmatrix} \mathbf{t}_1 \\ \mathbf{t}_2 \end{Bmatrix} = \Lambda^t \begin{Bmatrix} \mathbf{e}_1 \\ \mathbf{e}_2 \end{Bmatrix}, \quad \text{where } \Lambda := \begin{bmatrix} \cos\theta & -\sin\theta \\ \sin\theta & \cos\theta \end{bmatrix}. \tag{3.2}$$

Note that the floating basis $\{\mathbf{a}_1, \mathbf{a}_2\}$ plays no role in the present formulation.

3.2 Motivation: Kinetic Energy. We show that the kinetic energy of the system relative to the inertial basis reduces to the standard quadratic uncoupled form. To see this, note that from equation (3.2) the rate of change of the moving vectors $\{\mathbf{t}_1, \mathbf{t}_2\}$ is given by

$$\dot{\mathbf{t}}_1 = \dot{\theta}\mathbf{t}_2, \quad \dot{\mathbf{t}}_2 = -\dot{\theta}\mathbf{t}_1. \tag{3.4}$$

Hence, the time derivative $\dot{\boldsymbol{\phi}}$ of the position vector $\boldsymbol{\phi}$ is obtained as

$$\begin{aligned} \dot{\boldsymbol{\phi}} &= \dot{\boldsymbol{\phi}}_0 - X_2\dot{\theta}\mathbf{t}_1, \\ \dot{\boldsymbol{\phi}}_0 &= \dot{u}_1\mathbf{e}_1 + \dot{u}_2\mathbf{e}_2. \end{aligned} \tag{3.5}$$

It follows from equation (3.5) that $\|\dot{\boldsymbol{\phi}}\|^2 := \dot{\phi}_1^2 + \dot{\phi}_2^2$ has the expression

$$\|\dot{\boldsymbol{\phi}}\|^2 = [\dot{u}_1^2 + \dot{u}_2^2] + X_2^2\dot{\theta}^2 - 2\dot{\theta}X_2(\cos\theta\dot{u}_1 + \sin\theta\dot{u}_2). \tag{3.6}$$

Upon integrating $\rho(X_1, X_2)\|\dot{\boldsymbol{\phi}}\|^2$ over $[0, L] \times [-(h/2), h/2]$, we arrive at the following expression for the kinetic energy of the system

$$K = \frac{1}{2}\int_{[0,L]} [A_\rho(\dot{u}_1^2 + \dot{u}_2^2) + I_\rho\dot{\theta}^2]dX_1. \tag{3.7a}$$

Here, as in equation (2.13), the inertia coefficients A_ρ and I_ρ are given by equation (2.14).

Remark 3.1. The case of a flexible beam attached to a rigid body considered in Levinson and Kane (1981) can be readily accommodated within the present formulation by modifying expression (3.7*a*) for the kinetic energy. Let m_R be the mass of the rigid body, and I_R its inertia relative to an axis parallel to $\mathbf{e}_3 \equiv \mathbf{t}_3$ and passing through the connecting point with the beam. The kinetic energy of the composite system, then, is given by

$$K_{\text{total}} = K + \frac{1}{2}m_R\|\dot{\boldsymbol{\phi}}_0(0,t)\|^2 + \frac{1}{2}I_R\dot{\theta}^2(0,t) \tag{3.7b}$$

where K is given by (3.7*a*).

Remark 3.2. It is noted that expression (2.13) for the kinetic energy in the shadow beam approach may be exactly recovered from equation (3.7) simply by employing the coordinate transformation

$$\begin{Bmatrix} X_1 + u_1 \\ u_2 \end{Bmatrix} = \begin{bmatrix} \cos\psi & -\sin\psi \\ \sin\psi & \cos\psi \end{bmatrix} \begin{Bmatrix} X_1 + \tilde{u}_1 \\ \tilde{u}_2 \end{Bmatrix} \tag{3.8}$$

That is, the expression for the kinetic energy of the system is independent of any particular assumption on the magnitude of the strain field.

3.3 Potential Energy: Invariant Strain Measures. Within the context of large strains, a physically reasonable definition of the strain field in the beam is also provided in vectorial form by expression (2.4)

$$\boldsymbol{\gamma} := \boldsymbol{\phi}_0' - \mathbf{t}_1, \quad \boldsymbol{\kappa} := \theta'\mathbf{t}_3. \tag{3.9a}$$

The physical interpretation of $\boldsymbol{\gamma}$ is clear as shown in Fig. 3.1. $\boldsymbol{\gamma}$ measures the difference between the slope of the deformed axis of the beam and the normal to the cross section defined by $\mathbf{t}_1$, and $\boldsymbol{\kappa}$ is the rate of rotation of the cross section along the undeformed length of the beam. In component form, relative to the inertial frame we have from equation (3.1*b*) the following expression for $\boldsymbol{\gamma}$

$$\boldsymbol{\gamma} = \gamma_1\mathbf{e}_1 + \gamma_2\mathbf{e}_2 \equiv [(1 + u_1') - \cos\theta]\mathbf{e}_1 + [u_2' - \sin\theta]\mathbf{e}_2 \tag{3.9b}$$

Alternatively, relative to the *moving vectors* $\{\mathbf{t}_1, \mathbf{t}_2\}$, from relation (3.2) we have the following expression

$$\boldsymbol{\gamma} = \Gamma_1\mathbf{t}_1 + \Gamma_2\mathbf{t}_2, \tag{3.10a}$$

where

$$\begin{Bmatrix} \Gamma_1 \\ \Gamma_2 \end{Bmatrix} = \Lambda^t \begin{Bmatrix} 1 + u_1' - \cos\theta \\ u_2' - \sin\theta \end{Bmatrix}. \tag{3.10b}$$

The analogy between expressions (2.4*a*,*b*,*c*) and (3.9*a*)-(3.9*b*) should be noted. We now assume the same expression for the potential energy, relative to the moving frame $\{\mathbf{t}_1, \mathbf{t}_2\}$, as the one considered in the small strain shadow beam approach discussed in Section 2. Accordingly, we set

$$\begin{aligned} \Pi := \frac{1}{2}\int_{[0,L]} \{EA\Gamma_1^2 + GA_s\Gamma_2^2 + EI(\theta')^2\}dS \\ + \Pi_{EXT} - T(t)\theta(0,t) \end{aligned} \tag{3.11}$$

Remark 3.3. The components of the strain $\boldsymbol{\gamma}$ in the basis $\{\mathbf{t}_1, \mathbf{t}_2\}$ denoted by $[\Gamma_1\ \Gamma_2]^t$ are invariant under superposed rigid body motions on the beam. One can see this by considering the rigid body motion composed of a superposed translation $\mathbf{c}(t)$, and a superposed rotation $\beta(t)$ represented by the orthogonal transformation matrix

$$\mathbf{Q}(t) := \begin{bmatrix} \cos\beta & -\sin\beta \\ \sin\beta & \cos\beta \end{bmatrix}. \tag{3.12a}$$

The transformed quantities in the expression of Γ_i in equations (3.10) above are as follows

$$\begin{aligned} \boldsymbol{\phi}_o^+(X_1,t) &= \mathbf{c}(t) + \mathbf{Q}(t)\boldsymbol{\phi}_o(X_1,t), \\ \boldsymbol{\phi}_o^{+\prime} &:= \phi_{o1}^{+\prime}\mathbf{e}_1 + \phi_{o2}^{+\prime}\mathbf{e}_2 = \mathbf{Q}\boldsymbol{\phi}_o', \end{aligned} \tag{3.12b}$$

$$\text{i.e., } \begin{Bmatrix} \phi_{o1}^{+\prime} \\ \phi_{o2}^{+\prime} \end{Bmatrix} = \mathbf{Q} \begin{Bmatrix} 1 + u_1' \\ u_2' \end{Bmatrix}, \tag{3.12c}$$

$$\Lambda^+ = \mathbf{Q}\Lambda, \tag{3.12d}$$

Since $\mathbf{t}_1^+ = \cos(\beta+\theta)\mathbf{e}_1 + \sin(\beta+\theta)\mathbf{e}_2$, it follows that

$$\boldsymbol{\gamma}^+ := \Gamma_1^+\mathbf{t}_1^+ + \Gamma_2^+\mathbf{t}_2^+ = \boldsymbol{\phi}_o^{+\prime} - \mathbf{t}_1^+, \tag{3.13a}$$

where

$$\begin{Bmatrix} \Gamma_1^+ \\ \Gamma_2^+ \end{Bmatrix} = \Lambda^{+t} \left[\begin{Bmatrix} \phi_{o1}^{+\prime} \\ \phi_{o2}^{+\prime} \end{Bmatrix} - \begin{Bmatrix} \cos(\beta+\theta) \\ \sin(\beta+\theta) \end{Bmatrix} \right] \equiv \begin{Bmatrix} \Gamma_2 \\ \Gamma_1 \end{Bmatrix}. \tag{3.13b}$$

The invariance under superposed rigid body motions of the *curvature* κ follows at once in the plane case from expression (3.9*a*). This invariance property of the strain measures is essential for the success of the proposed approach.

Remark 3.4. It can be shown that definition (3.9*a*) and expressions (3.9*b*), (3.10) follow from a rigorous argument based on the equivalence of the stress power for the general three dimensional theory with the reduced stress power of the (finite strain) beam theory; see Antman (1972, 1974) and Simo (1985).

Remark 3.5. We shall be concerned only with spatially fixed loads, which do not depend on the deformed configuration, as opposed to follower loads that are configuration dependent. Simo and Vu-Quoc (1985) give a treatment of follower loads in the general context of the three-dimensional finite strain beam. Accordingly, the potential of the distributed loading in $(0, L)$ is given by

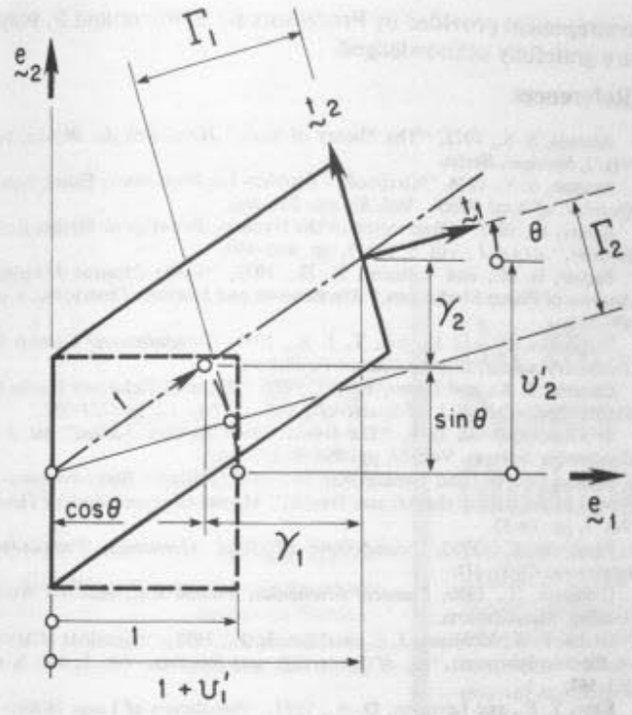

Fig. 3.1 Physical interpretation of the strain components of a beam in the finite strain case

$$\Pi_{EXT} = \int_{[0,L]} [\bar{\mathbf{m}} \cdot \theta \mathbf{e}_3 + \bar{\mathbf{n}} \cdot \boldsymbol{\phi}_0] dX_1 \tag{3.14}$$

Here, $\bar{\mathbf{n}}(X_1, t) := \bar{n}_1(X_1, t)\mathbf{e}_1 + \bar{n}_2(X_1, t)\mathbf{e}_2$ and $\bar{\mathbf{m}}(X_1, t) := \bar{m}(X_1, t)\mathbf{e}_3$ are the external force and torque per unit of reference length acting on the beam.

Remark 3.6. Dissipative mechanisms with viscous force proportional to the velocity can be readily accommodated in the formulation. To this end, the first variation of equation (2.15) is augmented by a velocity dependent dissipative term W_D defined by

$$W_D := -\int_{[t_1,t_2]} \int_{[0,L]} [\mathbf{n}_D \cdot \delta\boldsymbol{\phi}_0 + \mathbf{m}_D \cdot \delta\theta \mathbf{e}_3] dX_1 dt, \tag{3.15}$$

where $\delta\boldsymbol{\phi}_0$ and $\delta\theta\mathbf{e}_3$ denote arbitrary variations, and $\mathbf{n}_D$ and $\mathbf{m}_D$ are the velocity proportional viscous force and torque. For simplicity, we assume the expressions

$$\mathbf{n}_D := \mu A_\rho \dot{\boldsymbol{\phi}}_0, \quad \mathbf{m}_D := \mu I_\rho \dot{\theta} \mathbf{e}_3. \tag{3.16}$$

In the linear case this dissipative mechanism is often referred to as mass proportional damping, and becomes progressively ineffective in the high frequency range of the response. Alternative dissipative mechanisms typically involve inelastic constitutive behavior, e.g., viscoelastic response.

3.4 Equations of Motion: Uncoupled Inertia Terms. As in Section 2, the equations of motion governing the evolution of the system may be systematically obtained from Hamilton's principle. Standard manipulations yield the final result

$$A_\rho \ddot{\boldsymbol{\phi}}_0 + \mu A_\rho \dot{\boldsymbol{\phi}}_0 - \left[\mathbf{\Lambda C \Lambda}^t \begin{Bmatrix} 1 + u_1' - \cos\theta \\ u_2' - \sin\theta \end{Bmatrix} \right]' - \bar{n} = 0, \tag{3.17a}$$

$$I_\rho \ddot{\theta} + \mu I_\rho \dot{\theta} - EI\theta'' - \begin{Bmatrix} -u_2' \\ 1 + u_1' \end{Bmatrix}^t \mathbf{\Lambda C \Lambda}^t \begin{Bmatrix} 1 + u_1' - \cos\theta \\ u_2' - \sin\theta \end{Bmatrix} - \bar{m} = 0. \tag{3.17b}$$

We recall that $\mathbf{A}$ and $\mathbf{C}$ are given by

$$\mathbf{C} := \begin{bmatrix} EA & 0 \\ 0 & GA_s \end{bmatrix}, \quad \mathbf{\Lambda} := \begin{bmatrix} \cos\theta & -\sin\theta \\ \sin\theta & \cos\theta \end{bmatrix}. \tag{3.17c}$$

Equations (3.17*a*,*b*) comprise the system of nonlinear partial differential equations governing the response of the system. Note that these nonlinear equations are linear in the time derivative terms.

To define the natural boundary conditions, and for subsequent developments, we introduce the notation

$$\begin{Bmatrix} n_1 \\ n_2 \end{Bmatrix} := \mathbf{\Lambda C \Lambda}^t \begin{Bmatrix} 1 + u_1' - \cos\theta \\ u_2' - \sin\theta \end{Bmatrix}, \quad m := EI\theta'. \tag{3.18}$$

Here, $\mathbf{n}(X_1, t) := n_1(X_1, t)\mathbf{e}_1 + n_2(X_1, t)\mathbf{e}_2$ and $\mathbf{m}(X_1, t) := m(X_1, t)\mathbf{e}_3$ represent the internal force and internal moment acting on a deformed cross section of the beam. For the robot arm in Fig. 3.1 we have the following natural boundary conditions

$$\mathbf{m}(0,t) = T(t)\mathbf{e}_3, \quad \mathbf{m}(L,t) = \mathbf{n}(L,t) = \mathbf{0}. \tag{3.19}$$

These boundary conditions follow automatically from Hamilton's principle and the appropriate expression for Π_{EXT}.

3.5 Conservation of Global Momenta. Within the proposed approach *global* linear and angular momenta are automatically satisfied, and do not provide an additional constraint. This is in contrast with the shadow beam approach in which the basic equations of motion (2.16) must be supplemented by the global angular momentum condition (2.17) for the evolution of the system to be completely determined. To verify conservation of global linear and angular momenta we rewrite equations (3.17*a*,*b*) with the aid of equation (3.19) as

$$\dot{\mathbf{L}} - \mathbf{n}' - \bar{\mathbf{n}}' = \mathbf{0}, \quad \dot{\mathbf{H}} - \mathbf{m}' - \boldsymbol{\phi}_0' \times \mathbf{n} - \bar{\mathbf{m}} = \mathbf{0}. \tag{3.20a}$$

Here $\mathbf{L}(X_1, t)$ denotes the linear momentum per unit length, and $\mathbf{H}(X_1, t)$ the angular momentum per unit length relative to the centroid of the deformed cross section. Using equation (3.1) we have

$$\mathbf{L} := \int_{\left[-\frac{h}{2}, \frac{h}{2}\right]} \rho \dot{\boldsymbol{\phi}} dX_2 = A_\rho \dot{\boldsymbol{\phi}}_0,$$

$$\mathbf{H} := \int_{\left[-\frac{h}{2}, \frac{h}{2}\right]} \rho [\boldsymbol{\phi} - \boldsymbol{\phi}_0] \times \dot{\boldsymbol{\phi}} dX_2 = I_\rho \dot{\theta} \mathbf{e}_3, \tag{3.20b}$$

where $\mathbf{e}_3 := \mathbf{e}_1 \times \mathbf{e}_2$. The global linear and angular momentum of the system denoted by $\mathbb{L}(t)$ and $\mathbb{H}(t)$, respectively, are defined as

$$\mathbb{L}(t) := \int_{[0,L] \times \left[-\frac{h}{2}, \frac{h}{2}\right]} \rho \dot{\boldsymbol{\phi}} \, dX_1 dX_2,$$

$$\mathbb{H}(t) := \int_{[0,L] \times \left[-\frac{h}{2}, \frac{h}{2}\right]} \rho \boldsymbol{\phi} \times \dot{\boldsymbol{\phi}} \, dX_1 dX_2. \tag{3.21}$$

Making use of the identity $\boldsymbol{\phi} \times \dot{\boldsymbol{\phi}} = (\boldsymbol{\phi} - \boldsymbol{\phi}_0) \times \dot{\boldsymbol{\phi}} + \boldsymbol{\phi}_0 \times \dot{\boldsymbol{\phi}}$ the global angular momentum is expressed as

$$\mathbb{H}(t) = \int_{[0,L]} [\mathbf{H} + \boldsymbol{\phi}_0 \times \mathbf{L}] dX_1, \tag{3.22}$$

where $\mathbf{L}(X_1,t)$ and $\mathbf{H}(X_1,t)$ are given in equation (3.20*b*). Differentiating equation (3.22) and using equation (3.20*a*), we obtain the following condition involving the applied load and boundary conditions

$$\dot{\mathbb{H}} = [\mathbf{m} + \boldsymbol{\phi}_0 \times \mathbf{n}] \Big|_{X_1 = 0}^{X_1 = L} + \int_{[0,L]} [\bar{\mathbf{m}} + \boldsymbol{\phi}_0 \times \bar{\mathbf{n}}] dX_1. \tag{3.23}$$

Condition (3.23) states that the resultant torque of the applied

loading equals the rate of change of the total angular momentum. Similarly, for the global linear momentum we obtain

$$\dot{\mathbf{H}}\mathbf{L} = \mathbf{n}\Big|_{X_1=0}^{X_1=L} + \int_{[0,L]} \hat{\mathbf{n}} dX_1, \tag{3.24}$$

which states that the resultant force of the applied loads equals the rate of change of the global linear momentum. Equations of motion (3.20*a*) along with definitions (3.20*b*) are general, and remain valid in the three dimensional theory. Thus, the foregoing discussion leading to expressions (3.23) and (3.24) is not only restricted to the plane case.

4 Concluding Remarks

In this paper, we have presented a new approach to the dynamics of a plane beam under large overall motions. The essence of this approach is the fully nonlinear plane beam theory that can account for finite rotations as well as finite strains. The appropriate strain measures in the beam theory are invariant under superposed rigid body motion; such invariance is the necessary ingredient to the success of the present approach. The motion of the beam is completely referred to the inertial frame. We thus obtain the expression of the inertia term in the equations of motion simply as mass times acceleration. By contrast, in the shadow beam approach, one obtains a nonlinear and highly coupled inertia operator; hence a special computer code must be devised to solve the resulting system. In our approach, the inherent nonlinear character of the problem is transferred to the stiffness part of the equations of motion; this results in equations of motion that arise typically in nonlinear structural dynamics. As demonstrated in Part II of this paper, the dynamics of flexible beams under large overall motions can be analyzed in any existing nonlinear finite element program. Without alteration in the formulation, one can apply this approach to the dynamics of a system of flexible beams connected by hinges, as shown by our numerical examples. In addition, the approach proposed in this paper can be readily extended to accommodate inelastic constitutive behavior, and can be used to treat a wide range of problems including the dynamic analysis of an earth-orbiting satellite composed of beam elements. Finally we note that, conceptually, the proposed approach readily carries over to the fully three dimensional case. Further comments on possible extensions of the proposed methodology are given in part II of this paper.

Acknowledgments

We thank Professor R. L. Taylor, the developer of FEAP, for his helpful discussions. This work was performed under the auspices of the Air Force Office of Scientific Research, grant No. AFOSR-83-0361. This support as well as the encouragement provided by Professors K. S. Pister and E. Polak are gratefully acknowledged.

References

Antman, S. S., 1972, "The Theory of Rod," *Handbuch der Physics*, Vol. VIa/2, Springer, Berlin.

Antman, S. S., 1974, "Kirchhoff's Problem for Nonlinearly Elastic Rods," *Quart. J. of Appl. Math.*, Vol. 32, pp. 221–240.

Ashley, H., 1967, "Observation of the Dynamic Behavior of Flexible Bodies in Orbit," *AIAA J.*, Vol. 5, No. 3, pp. 460–469.

Baghat, B. M., and Willmert, K. D., 1973, "Finite Element Vibrational Analysis of Planar Mechanism," *Mechanisms and Machine Theory*, Vol. 8, pp. 497–516.

Belytschko, T., and Hughes, T. J. R., 1983, *Computational Methods For Transient Analysis*, Elsevier Science Publishers.

Canavin, J. R., and Likins, P. W., 1977, "Floating Reference Frames for Flexible Spacecrafts," *J. of Spacecraft*, Vol. 14, No. 12, pp. 724–732.

de Veubeke, B. J., 1976, "The Dynamics of Flexible Bodies," *Int. J. of Engineering Sciences*, Vol. 14, pp. 895–913.

Erdman, A. G., and Sandor, G. N., 1972, "Kineto-Elastodynamics—A Review of the State of the Art and Trends," *Mechanisms and Machine Theory*, Vol. 7, pp. 19–33.

Fung, Y. C., 1965, *Foundations of Solid Mechanics*, Prentice-Hall, Englewood Cliffs, NJ.

Goldstein, H., 1980, *Classical Mechanics*, Second Ed., Addison Wesley, Reading, Massachusetts.

Grotte, P. B., McMunn, J. C., and Gluck, R., 1971, "Equations of Motion of Flexible Spacecraft," *J. of Spacecraft and Rockets*, Vol. 8, No. 6, pp. 561–567.

Kane, T. R., and Levinson, D. A., 1981, "Simulation of Large Motions of Nonuniform Beams in Orbit: Part II—The Unrestrained Beam," *The J. of the Astronautical Sciences*, Vol. 29, No. 3, pp. 213–244.

Kane, T. R., Likins, P. W., and Levinson, D. A., 1983, *Spacecraft Dynamics*, McGraw-Hill, New York.

Kumar, V. K., and Bainum, P. M., 1980, "Dynamics of a Flexible Body in Orbit," *J. of Guidance and Control*, Vol. 3, No. 1, pp. 90–91.

Laskin, R. A., Likins, P. W., and Longman, R. W., 1983, "Dynamical Equations of a Free-Free Beam Subject to Large Overall Motions," *The J. of the Astronautical Sciences*, Vol. 31, No. 4, pp. 507–528.

Levinson, D. A., and Kane, T. R., 1981, "Simulation of Large Motions of Nonuniform Beams in Orbit: Part I—The Cantilever Beam," *The J. of the Astronautical Sciences*, Vol. 29, No. 3, pp. 245–276.

Likins, P. W., 1974, "Analytical Dynamics and Nonrigid Spacecraft Simulation," *Jet Propulsion Laboratory, Technical Report 32-1593*, California Institute of Technology.

Petzold, L. R., 1982, "Differential/Algebraic Equations are Not ODE's," *SIAM J. Sci. Stat. Comput.*, Vol. 3, No. 3, pp. 367–384.

Reissner, E., 1972, "On a One Dimensional Finite Strain Beam: The Plane Problem," *J. Appl. Math. Phys.*, Vol. 23, pp. 795–804.

Reissner, E., 1973, "On a One-Dimensional Large-Displacement, Finite-Strain Beam Theory," *Studies in Applied Math*, Vol. 52, pp. 87–95.

Reissner, E., 1981, "On Finite Deformations of Space-Curved Beams," ZAMP, Vol. 32, pp. 734–744.

Simo, J. C., 1985, "A Finite Strain Beam Formulation. The Three Dimensional Dynamic Problem. Part I," *Comp. Meth. Appl. Mech. Engrg.*, Vol. 49, pp. 55–70.

Simo, J. C., and Vu-Quoc, L., 1985, "Three Dimensional Finite Strain Rod Model. Part II: Computational Aspects," *Electronics Research Laboratory Memorandum No. UCB/ERL M85/31*, University of California, Berkeley, April. (Submitted for publication.)

Simo, J. C., and Vu-Quoc, L., 1986, *The Role of Nonlinear Theories in the Dynamics Analysis of Rotating Structures*, Electronics Research Laboratory Memorandum UCB/ERL M86/10, University of California, Berkeley, January.

Song, J. O., and Huag, E. J., 1980, "Dynamic Analysis of Planar Flexible Mechanism," *Comp. Meth. Appl. Mech. Engrg.*, Vol. 24, pp. 359–381.

Winfrey, R. C., 1971, "Elastic Link Mechanism Dynamics," *ASME J. of Engineering for Industry*, Vol. 93, No. 1, pp. 268–272.

J. C. Simo[1]
Applied Mechanics Division,
Stanford University,
Stanford, CA 94305

L. Vu-Quoc
Structural Engineering and Structural
Mechanics Division,
University of California,
Berkeley, CA 94720

On the Dynamics of Flexible Beams Under Large Overall Motions—The Plane Case: Part II

The numerical treatment of the methodology proposed in Part I of this paper is considered in detail. Unlike traditional approaches, a Galerkin spatial discretization of the equations of motion, now referred to the inertial frame, yields the standard form of nonlinear structural dynamics: $\mathbf{M}\ddot{\mathbf{q}} + \mathbf{D}\dot{\mathbf{q}} + \mathbf{P}(\mathbf{q}) = \mathbf{F}$, *with* $\mathbf{M}$ *and* $\mathbf{D}$ *constant matrices. Numerical examples that involve finite vibrations coupled with large overall motions are presented. These simulations also demonstrate the capability of the present formulation in handling* multibody dynamics.

1 Numerical Approximation: Galerkin Method

In this section we discuss the numerical treatment of the nonlinear partial differential equations developed in Section 3 of Part I. The basic strategy is to perform a Galerkin discretization in the spatial variable leading to the standard system of ODE's in the time variable characteristic of nonlinear structural dynamics. This system may then be solved discretely using standard time stepping algorithms (e.g., the Newmark family). The finite element method provides an established technique for constructing the (spatial) basis functions necessary to perform the Galerkin discretization. Expressions of the matrices resulting from the application of this procedure are given in the appendix.

1.1 Weak Form of Equations of Motion—Spatial Discretization. The equations of motion (3.14) of Part I may be put in the following form

$$\mathbf{I}\ddot{\mathbf{d}}(X_1,t) + \Delta\dot{\mathbf{d}}(X_1,t) + \mathbf{P}[\mathbf{d}(X_1,t) = \mathbf{f}(X_1,t), \qquad (1.1a)$$

where

$$\mathbf{I} := \mathrm{Diag}[A_\rho, A_\rho, I_\rho],\ \Delta := \mathrm{Diag}[\mu A_\rho, \mu A_\rho, \mu I_\rho], \qquad (1.1b)$$

$$\mathbf{d}(X_1,t) := \begin{Bmatrix} X_1 + u_1(X_1,t) \\ u_2(X_1,t) \\ \theta(X_1,t) \end{Bmatrix}, \quad \mathbf{f}(X_1,t) := \begin{Bmatrix} \bar{n}_1(X_1,t) \\ \bar{n}_2(X_1,t) \\ \bar{m}(X_1,t) \end{Bmatrix}$$

Equation (1.1a) is a nonlinear partial differential equation in the generalized vector $\mathbf{d}(X_1, t) \in V_1$, where V_1 is the space of admissible (generalized) displacements.[2] This equation is linear in the terms involving time derivatives, i.e., the acceleration $\ddot{\mathbf{d}}$ in the first term and the velocity $\dot{\mathbf{d}}$ in the second term. The third term $\mathbf{P}[\mathbf{d}]$, on the other hand, is a nonlinear differential operator in the space variable $X_1 \in (0,L)$. This nonlinearity results from the coupling between large overall motions and (finite) strain deformations in the beam. Concerning the applied load $\bar{\mathbf{n}}$ and $\bar{m}$, see remark 3.5. The weak form $G(\mathbf{d},\boldsymbol{\eta})$ of equation (1.1a) is obtained by integrating over the spatial domain $(0,L) \subset \mathbf{R}$ the dot product of this equation with an arbitrary weighting function $\boldsymbol{\eta} \in V_2$.[3] That is

$$G(\mathbf{d},\boldsymbol{\eta}) := \int_{[0,L]} \boldsymbol{\eta}'[\mathbf{I}\,\ddot{\mathbf{d}} + \Delta\dot{\mathbf{d}} + \mathbf{P}[\mathbf{d}] - \mathbf{f}]dX_1 = 0, \forall \boldsymbol{\eta} \in V_2 \qquad (1.2)$$

The final expression is obtained from (1.2) by integration by parts on the spatial derivatives entering $\mathbf{P}[\mathbf{d}]$, so that only *first order spatial derivatives* are involved in $G(\mathbf{d},\boldsymbol{\eta})$. We refer to the appendix for the details. The displacements $\mathbf{d}(X_1,t)$ and the weighting function $\boldsymbol{\eta}(X_1)$ are then interpolated in the spatial variable X_1 according to

$$\mathbf{d}(X_1,t) \cong \sum_{I=1}^{N} \Psi_I(X_1)\mathbf{q}_I(t),$$

$$\boldsymbol{\eta}(X_1) \cong \sum_{I=1}^{N} \Psi_I(X_1)\boldsymbol{\eta}_I \qquad (1.3)$$

Upon introducing the spatial discretization (1.3) of $\mathbf{d}(X_1,t)$ and of $\boldsymbol{\eta}(X_1)$ into the weak form (1.2), we obtain the semi-discrete equation of motion in matrix form

$$\mathbf{M}\ddot{\mathbf{q}}(t) + \mathbf{D}\dot{\mathbf{d}}(t) + \mathbf{P}(\mathbf{q}(t)) = \mathbf{F}(t) \qquad (1.4)$$

[1] Formerly at the University of California, Berkeley.

Contributed by the Applied Mechanics Division for presentation at the Winter Annual Meeting, Anaheim, CA, December 7–12, 1986, of The American Society of Mechanical Engineers.

Discussion on this paper should be addressed to the Editorial Department, ASME, United Engineering Center, 345 East 47th Street, New York, N.Y. 10017, and will be accepted until two months after final publication of the paper itself in the JOURNAL OF APPLIED MECHANICS. Manuscript received by ASME Applied Mechanics Division, September 23, 1985; final revision, May 7, 1986. Paper No. 86-WA/APM-42.

[2] A possible choice for V_1 could be $V_1 := \{\mathbf{d} \in [H^1(0,L) \times C^\infty[0,\infty)]^3 \mid u_1|_{x_1=0} = u_2|_{x_1=0} = 0, \text{ and } \theta|_{x_1=0} = 0\}$

[3] V_2 could be chosen to be $V_2 := \{\boldsymbol{\eta} \in [H^1(0,L)]^3 \mid$ with appropriate boundary conditions for $\boldsymbol{\eta}$ such that $\eta_1 n_1 + \eta_2 n_2 + \eta_3 m = 0$ at the boundaries$\}$

where $\mathbf{M}$ and $\mathbf{D}$ are constant mass and damping matrices, respectively, $\mathbf{q}(t) := [\mathbf{q}_1(t), \ldots, \mathbf{q}_N(t)]^t$ denotes the generalized displacement vector, $\mathbf{P}(\mathbf{q}(t))$ the vector of internal forces depending on $\mathbf{q}(t)$, and $\mathbf{F}(t)$ the applied load vector. Details of the expressions of $\mathbf{M}$, $\mathbf{D}$, $\mathbf{P}(\mathbf{q}(t))$, and $\mathbf{F}(t)$ can be found in the appendix.

Remark 1.1. In the absence of dissipative mechanisms (e.g., damping) the system has a well defined energy function $H = K + \Pi$. The Galerkin procedure outlined above is then equivalent to a standard Raleigh-Ritz approximation based on $(1.3)_1$. See, e.g., Meirovitch (1970).

Remark 1.2. In the shadow beam approach restricted to small-strains, one may also use the modal superposition method to discretize spatially the displacements $[\bar{u}_1, \bar{u}_2]$ as in (1.3). For this purpose, consider equations (2.16) of Part I. One first eliminates $\bar{\alpha}$ from equation (2.16) using $(2.16)_2$. The semi-discrete equation of motion of the system is then obtained by projecting the resulting equations (2.16) onto the orthogonal basis of mode-shapes of the Euler-Bernoulli cantilever beam. However, no matter which discretization procedure is used, the resulting semi-discrete equations of motion system constitute a system of highly *coupled nonlinear differential algebraic equations* (DAE). The solution of this complete system of DAE's is not a trivial task, and requires a specially designed computer code (Benson and Hallquist, 1985). Numerical integration methods for DAE systems may be found in Gear (1971a,b), Petzold (1982), and Gear and Petzold (1984). The solution of the standard nonlinear structural dynamics equation (1.4), on the other hand, is much simpler and may be carried out using any nonlinear structural finite element code. A time stepping algorithm solution procedure will be outlined in the next section.

Remark 1.3. Multibody Dynamics. In Section 5, we will show through numerical examples that the proposed approach can be applied without alteration in the formulation to study the dynamics of a system of flexible bodies connected through hinges. It is indeed a simple matter to model such a system in a finite element program. The shadow beam approach, on the other hand, leads to a much more involved formulation, e.g., as in Hughes (1979), Likins (1974), Song and Haug (1980), and Sunada and Dubowsky (1980).

1.2 Time Stepping Scheme—Temporal Discretization. The semi-discrete equations of motion (1.4) can be trivially rephrased into the standard form of a system of nonlinear ODE's, $\dot{\mathbf{y}} = \mathbf{g}(\mathbf{y}, t)$, by setting $\mathbf{y} := \{\mathbf{q}, \dot{\mathbf{q}}\}$. This standard ODE system can be integrated by a variety of time stepping algorithms (Gear, 1971), which must be *consistent* with (1.4) and *stable* for some range of the time step. We refer to standard textbooks such as Gear (1971) and Richtmyer and Morton (1967) for precise definitions of these concepts. Two basic strategies in devising algorithms for (1.4) may be adopted:

(*a*) *Explicit schemes:* Typically, high accuracy may be achieved by employng high order methods. A classical example is furnished by the family of Runge-Kutta methods. It is well-known that the main drawback of explicit schemes is the severe limitation on the time step imposed by their restrictive stability characteristics.

(*b*) *Implicit scheme* typically possess very robust stability characteristics. Classical examples are the trapezoidal rule, which is the highest order A-stable method possible (Dahlquist, 1963), the stiffly stable methods of Gear (1971b), and the family of algorithms devised by Newmark (1959) and widely used in nonlinear structural dynamics (Belytschko and Hughes, 1983).

Here, motivated by stability considerations, attention is focused on the Newmark family of algorithms for solving (1.4), which includes the trapezoidal rule as a special case. The behavior and stability characteristics of the Newmark algorithm applied to *linear* problems is well established, e.g., see the analysis of Goudreau and Taylor (1973), and Hilber (1976). For completeness, we shall outline the basic steps involved in the numerical solution of (1.4) by the Newmark algorithm.

Let $\mathbf{q}_n$ denote the approximate solution to $\mathbf{q}(t_n)$ at time t_n. Similarly, $\mathbf{v}_n \cong \dot{\mathbf{q}}(t_n)$ and $\mathbf{r}_n \cong \ddot{\mathbf{q}}(t_n)$ represent the approximate velocity and acceleration at time t_n, respectively. Assume that the solution $\{\mathbf{q}_n, \mathbf{v}_n, \mathbf{r}_n\}$ at time t_n has already been obtained, i.e., the momentum equation (1.4) is satisfied at time t_n

$$\mathbf{M}\mathbf{r}_n + \mathbf{D}\mathbf{v}_n + \mathbf{P}(\mathbf{q}_n) = \mathbf{F}_n \tag{1.5}$$

where $\mathbf{F}_n \equiv \mathbf{F}(t_n)$. We now aim at satisfying the momentum equation (1.4) at time t_{n+1}, i.e.,

$$\mathbf{M}\mathbf{r}_{n+1} + \mathbf{D}\mathbf{v}_{n+1} + \mathbf{P}(\mathbf{q}_{n+1}) = \mathbf{F}_{n+1} \tag{1.6}$$

The Newmark time stepping algorithm defines the relationship between $\{\mathbf{q}_{n+1}, \mathbf{v}_{n+1}, \mathbf{r}_{n+1}\}$ according to the following formulae

$$\mathbf{r}_{n+1} = \frac{\mathbf{q}_{n+1} - \mathbf{q}_n}{h^2\beta} - \frac{\mathbf{v}_n}{h\beta} - \frac{\frac{1}{2} - \beta}{\beta}\mathbf{r}_n \tag{1.7a}$$

$$\mathbf{v}_{n+1} = \mathbf{v}_n + h[(1-\tau)\mathbf{r}_n + \tau\mathbf{r}_{n+1}], \tag{1.7b}$$

where $h := t_{n+1} - t_n$ denotes the time step size, and (β, τ) are the parameters of the Newmark algorithm. We note that $\beta = 0.25$ and $\tau = 0.5$ correspond to the trapezoidal rule; this choice of the parameters β and τ renders the algorithm *unconditionally stable* in the linear case,[4] and second order accurate. Substitution of equation (1.7*a*) into (1.6) yields a system of nonlinear algebraic equations in terms of $\mathbf{q}_{n+1}$.

The resulting nonlinear algebraic system may then be solved employing the classical Newton-Raphson method. Let $\mathbf{q}_{n+1}^{(i)}$ denote the value of $\mathbf{q}_{n+1}$ at iteration (i) of the Newton-Raphson algorithm, and $\Delta\mathbf{q}_{n+1}^{(i+1)}$ the incremental displacements. As an initial guess for $\{\mathbf{q}_{n+1}, \mathbf{v}_{n+1}, \mathbf{r}_{n+1}\}$, one may choose the starting value $\mathbf{q}_{n+1}^{(0)}$ to be the same as the converged value in the previous time increment, i.e., $\mathbf{q}_n$; the initial values $\mathbf{v}_{n+1}^{(0)}$ and $\mathbf{r}_{n+1}^{(0)}$ follow from the Newmark scheme (1.7):

$$\mathbf{q}_{n+1}^{(0)} = \mathbf{q}_n \tag{1.8a}$$

$$\mathbf{r}_{n+1}^{(0)} = -\left[\frac{\mathbf{v}_n}{h\beta} + \frac{\frac{1}{2} - \beta}{\beta}\mathbf{r}_n\right] \tag{1.8b}$$

$$\mathbf{v}_{n+1}^{(0)} = \mathbf{v}_n + h[(1-\tau)\mathbf{r}_n + \tau\mathbf{r}_{n+1}^{(0)}] \tag{1.8c}$$

At iteration (i) of the Newton-Raphson scheme, the linearization about $\mathbf{q}_{n+1}^{(i)}$ of the system of nonlinear algebraic equations yields

$$\left[\frac{1}{h^2\beta}\mathbf{M} + \frac{\tau}{h\beta}\mathbf{D} + \mathbf{K}_T(\mathbf{q}_{n+1}^{(i)})\right]\Delta\mathbf{q}_{n+1}^{(i+1)} = \mathbf{F}_{n+1} - \mathbf{M}\mathbf{r}_{n+1}^{(i)} - \mathbf{D}\mathbf{v}_{n+1}^{(i)} - \mathbf{P}(\mathbf{q}_{n+1}^{(i)}) \tag{1.9}$$

It should be noted here that while the mass matrix $\mathbf{M}$ is positive definite, the tangent stiffness matrix $\mathbf{K}_T(\mathbf{q}_{n+1}^{(i)})$ may be positive semi-definite. The system of equations (1.9) is of

[4] Roughly, the notion of stability corresponds to well-posedness of the semi-discrete problem. In the nonlinear case the appropriate concept of stability remains unsettled, and several notions of stability have been proposed (A-stability, spectral stability, stability in the energy sense, etc. . .). See, e.g., Belytschko and Hughes (1983), Gear (1971b), Chorin et al. (1978).

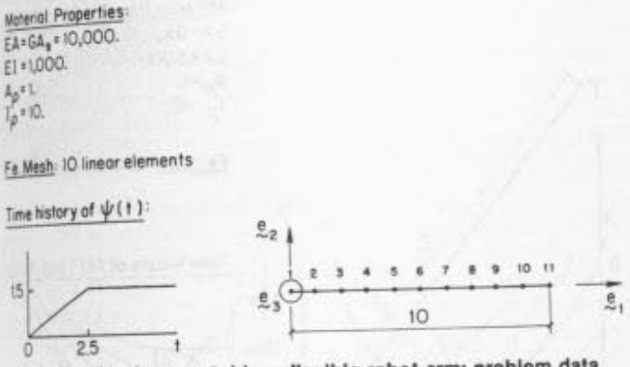

Fig. 1(a) Displacement driven flexible robot arm; problem data

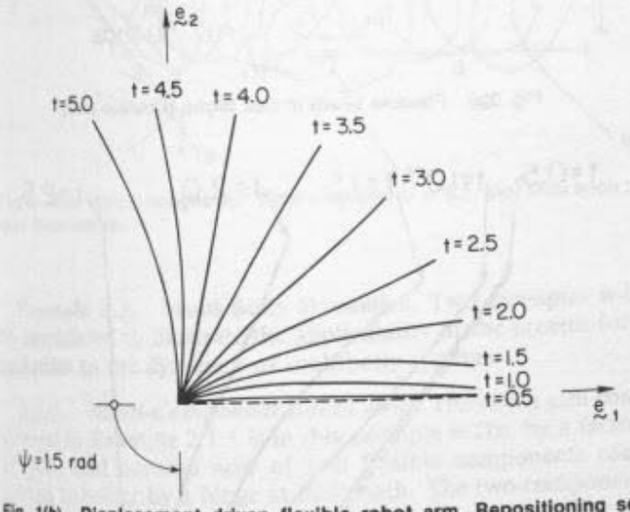

Fig. 1(b) Displacement driven flexible robot arm. Repositioning sequence to stop angle ψ = 1.5 rad. Time step size h = 0.5.

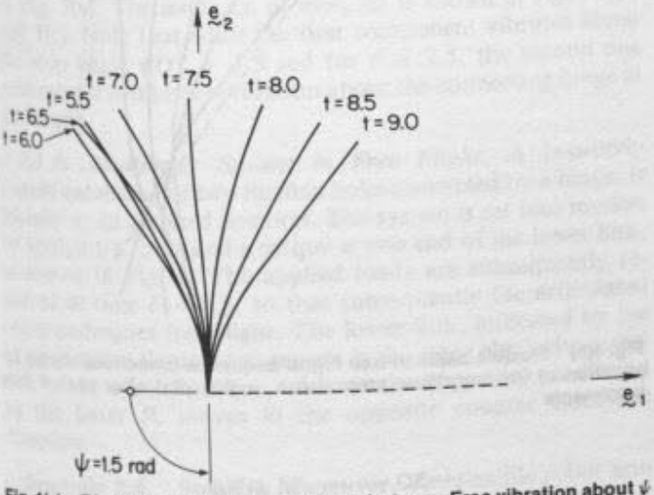

Fig. 1(c) Displacement driven flexible robot arm. Free vibration about ψ = 1.5 rad. Time step size h = 0.5.

the form $\hat{\mathbf{K}}\Delta\mathbf{q}_{n+1}^{(i+1)} = \hat{\mathbf{F}}$ where the matrix $\hat{\mathbf{K}}$ is banded, symmetric, and positive definite. Solving for $\Delta\mathbf{q}_{n+1}^{(i+1)}$, and updating $(\mathbf{q}_{n+1}^{(i)}, \mathbf{v}_{n+1}^{(i)}, \mathbf{r}_{n+1}^{(i)})$, we obtain the value of $\{\mathbf{q}_{n+1}, \mathbf{v}_{n+1}, \mathbf{r}_{n+1}\}$ at iteration $(i+1)$ as follows

$$\mathbf{q}_{n+1}^{(i+1)} = \mathbf{q}_{n+1}^{(i)} + \Delta\mathbf{q}_{n+1}^{(i+1)} \tag{1.10a}$$

$$\mathbf{v}_{n+1}^{(i+1)} = \mathbf{v}_{n+1}^{(i)} + \frac{\tau}{h\beta}\Delta\mathbf{q}_{n+1}^{(i+1)} \tag{1.10b}$$

$$\mathbf{r}_{n+1}^{(i+1)} = \mathbf{r}_{n+1}^{(i)} + \frac{1}{h^2\beta}\Delta\mathbf{q}_{n+1}^{(i+1)} \tag{1.10c}$$

The iterations are continued until convergence is attained within certain tolerance. A basic characteristic of Newton's iterative method is that the asymptotic rate of convergence is quadratic.

2 Numerical Simulations

In this section we present a series of numerical simulations that illustrate the formulation and numerical procedure discussed in Sections 3 of Part I. Our purpose is to exhibit:

(*a*) The simplicity of the numerical procedure. Essentially any existing nonlinear structural finite element dynamics code could be employed. Here we employ an extended version of the computer program FEAP developed by R. L. Taylor and documented in Zienkiewicz (1977), chapter 24.

(*b*) The capability of the proposed formulation to automatically handle *finite strains* superposed onto large overall rigid body motions. This includes flexible bodies in free flight. Viscous effects can also be accounted for easily in the formulation.

(*c*) The immediate applicability of the proposed approach to the dynanics of a system of interconnected flexible bodies without alteration of the formulation.

It is emphasized that no simplification is made in the simulations that follow in the sense that Coriolis and centrifugal effects as well as the inertia effect due to rotation are automatically accounted for. The deformed shapes in all figures reported in this paper are given at the *same* scale as the geometry of the beam, i.e., there is no magnification of the structural deformations.

In all simulations reported herein, the trapezoidal rule (Newmark algorithm with $\tau = 0.5$ and $\beta = 0.25$) was employed. Numerical operations were performed in double precision in a VAX 11/780 under the Berkeley UNIX 4.2 BSD operating system.

Example 2.1. Flexible Robot Arm. This simulation is concerned with the repositioning of a flexible beam rotating horizontally about a vertical axis passing through one end. The finite element mesh consists of 10 elements with linear isoparametric interpolation functions for both displacement and rotation. To avoid the well known "shear locking" phenomenon (Zienkiewicz, 1977), a uniformly reduced one-point Gauss quadrature is employed to integrate the tangent stiffness and residual. The mass matrix, however, is integrated exactly with two-point Gauss quadrature. Two cases are considered.

2.1.1. Displacement Driven Flexible Robot Arm. The geometry, material properties, finite element mesh, as well as the time step size used in the integration are given in Fig. 1(*a*). The robot arm is first repositioned to an angle of 1.5 *radians* from its initial position. This is achieved by prescribing the rotation angle $\psi(t) \equiv \theta(0, t)$ as a linear function of time, as shown in Fig. 1(*a*); the sequence of motion during this repositioning stage is depicted in Fig. 1(*b*). Once the rotation angle $\psi(t)$ is fixed at 1.5 rad for all time $t \geq 2.5$, the robot arm then undergoes finite vibrations as shown in Fig. 1(*c*).

2.1.2. Force Driven Flexible Robot Arm. The robot arm is now driven by a prescribed torque $T(t)$ applied at the axis of rotation $\mathbf{e}_3$, as shown in Fig. 2(*a*). The applied torque is removed at time $t = 2.5$; the robot arm then undergoes a torque-free motion. The simulation is terminated after completion of one revolution, as shown in Figs. 2(*b*) and 2(*c*).

Example 2.2. Flying Flexible Rod. A flexible rod with free ends, initially placed in an inclined position, is subject to a force and a torque applied simultaneously at one end, see Fig. 3(*a*). The applied force and torque are removed at the same time $t = 2.5$, so that the subsequent free flight of the rod exhibits a periodic tumbling pattern. It should be noted here that

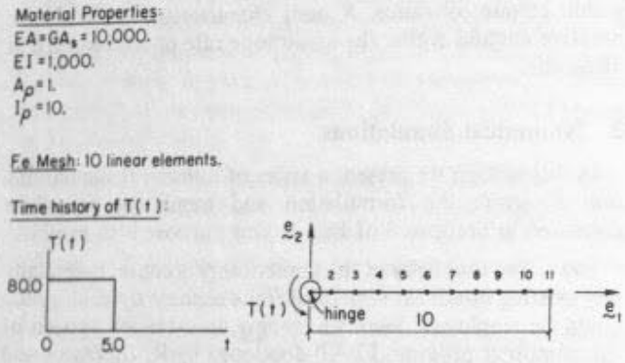

Fig. 2(*a*) Force driven flexible robot arm; problem data

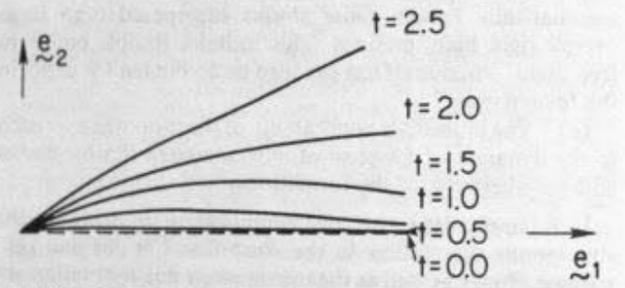

Fig. 2(*b*) Force driven flexible robot arm. Sequence of motion during application of torque. Time step size $h = 0.5$.

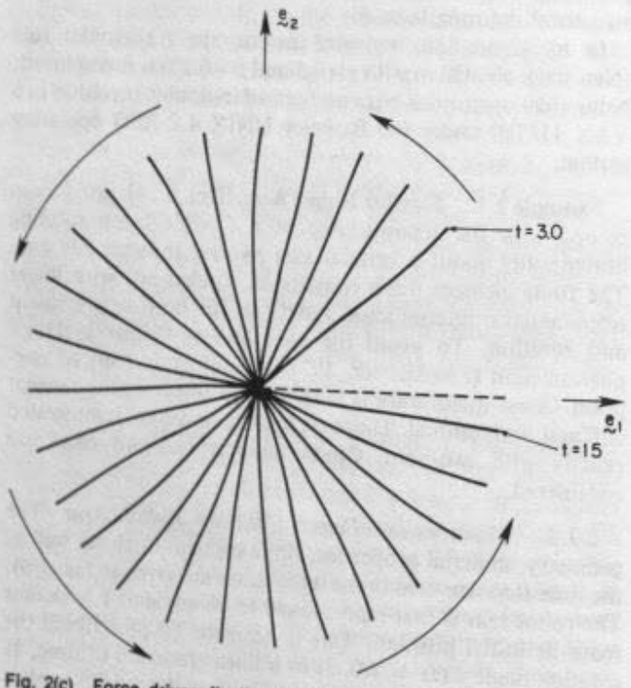

Fig. 2(*c*) Force driven flexible robot arm. Sequence of motion after removal of applied torque.

the boundary conditions (3.19) of Part I now become $\mathbf{m}(0,t) = \mathbf{m}(L,t) = \mathbf{n}(0,t) = \mathbf{n}(L,t) \equiv 0$ during the free flight stage. Two cases are considered.

2.2.1. Flexible Beam in Free Flight. The motion of the rod during application of loading is shown in Fig. 3(*b*). The stiffness of the rod is low enough to exhibit finite deformations. A close-up of the first two revolutions is shown in Fig. 3(*c*) while the entire sequence of motion is depicted in Fig. 3(*d*).

2.2.2. The "Flying Spaghetti." The bending stiffness EI of the rod is lowered by a factor of 5 relative to the simulation in 2.2.1. This dramatic reduction in stiffness results in the sequence of motions depicted in Fig. 4.

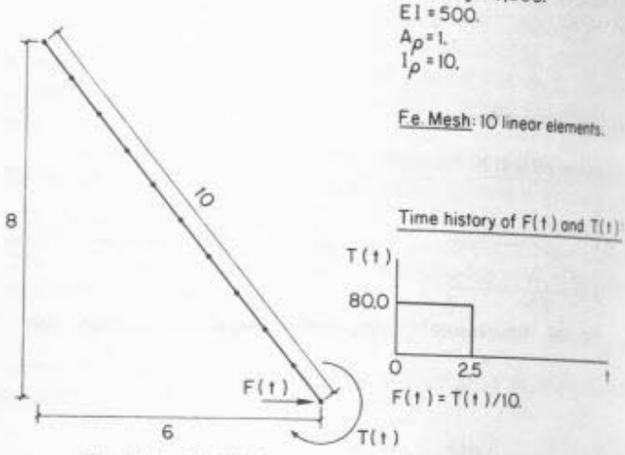

Fig. 3(*a*) Flexible beam in free flight; problem data.

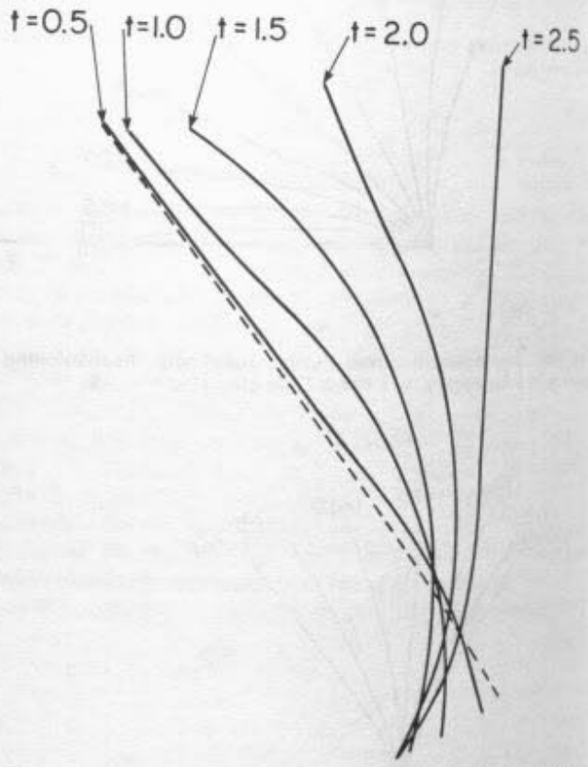

Fig. 3(*b*) Flexible beam in free flight. Sequence of motions during application of loading. Time step size $h = 0.1$, plot after each 5 time increments

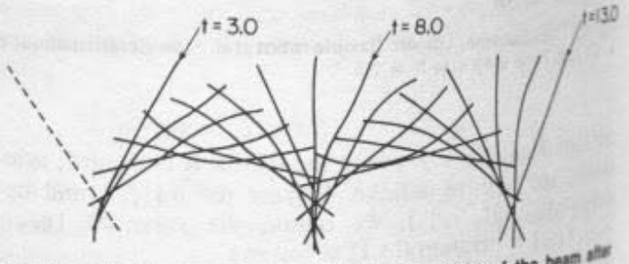

Fig. 3(*c*) Flexible beam in free flight. Free flight of the beam after removal of loading—close-up on the first 2 revolutions. Time step size $h = 0.1$, plot after each 5 time increments

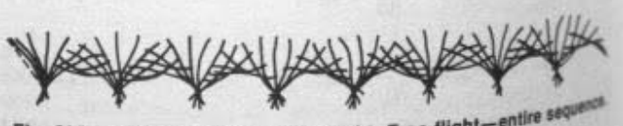

Fig. 3(*d*) Flexible beam in free flight. Free flight—entire sequence.

Material Properties:
$EA = GA_s = 10{,}000.$
$EI = 100.$
$A_\rho = 1.$
$I_\rho = 10.$

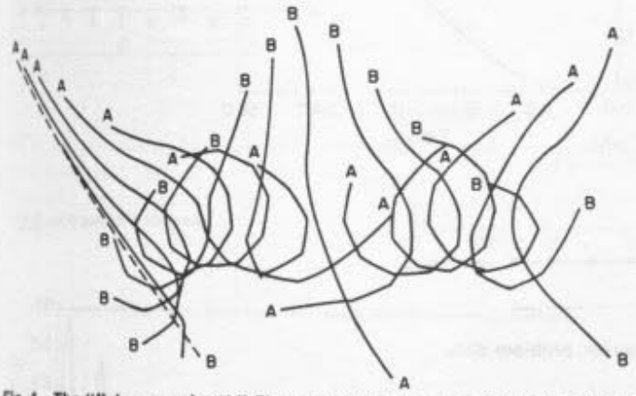

Fig. 4 The "flying spaghetti." Time step size $h = 0.1$, plot after each 5 time increments.

Example 2.3. Multi-Body Dynamics. Two examples will be considered to illustrate the applicability of the present formulation to the dynamics of multibody systems.

2.3.1. Multi-Component Robot Arm. The robot arm considered in Example 2.1.1 is in this example stiffer by a factor of 100, and consists now of two flexible components connected together by a hinge at midlength. The two-component robot arm is subjected to the same prescribe rotation $\psi(t) \equiv \theta(0, t)$ as in Example 2.1.1. The problem data are summarized in Fig. 5(*a*). The sequence of motions is shown in Figs. 5(*b*) and 5(*c*). Note that while the first component vibrates about the stop angle $\psi(t) = 1.5$ rad for $t \geq 2.5$, the second one undergoes a complete revolution about the connecting hinge at midlength.

2.3.2. Multibody System in Free Flight. A two-body system consisting of two flexible links connected by a hinge, is initially at an inclined position. The system is set into motion by applying a force and a torque at one end of the lower link, as shown in Fig. 6. The applied loads are subsequently removed at time $t = 0.5$, so that subsequently the articulated beam undergoes free flight. The lower link, indicated by the letter A in the figure, then moves in the same clockwise direction as the applied torque, whereas the upper link, indicated by the letter B, moves in the opposite counter clockwise direction.

Example 2.4. Spin-Up Maneuver. The flexible robot arm considered in Example 2.1.1 is now subject to a "spin-up" maneuver by prescribing the angle $\psi(t) \equiv \theta(0,t)$ for $t \in \mathbf{R}_+$ as follows

$$\psi(t) = \begin{cases} \dfrac{6}{15}\left[\dfrac{t^2}{2} + \left(\dfrac{15}{2\pi}\right)^2 \left(\cos\dfrac{2\pi t}{15} - 1\right)\right] \text{rad} & 0 \leq t \leq 15 \quad \text{sec} \\ (6t - 45)\ \text{rad} & t > 15 \quad \text{sec} \end{cases} \tag{2.1}$$

This type of motion was proposed in Kane et al. (1985) to illustrate how naive linearized approximations may lead to grossly inaccurate results, i.e., instability of a physically stable system. The motion is also of practical interest in applications such as helicopter rotor blades or aircraft propellers. The material properties and time history of $\psi(t)$ are shown in Fig.

Material Properties:
$EA = GA_s = 1{,}000{,}000.$
$EI = 100{,}000.$
$A_\rho = 1.$
$I_\rho = 1.$

Fe Mesh: 4 quadratic elements.

Time history of $\psi(t)$:

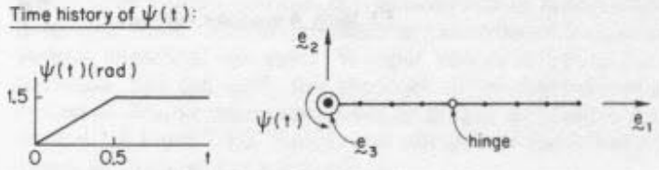

Fig. 5(*a*) Multibody dynamics: displacement driven, multi-component robot arm; problem data

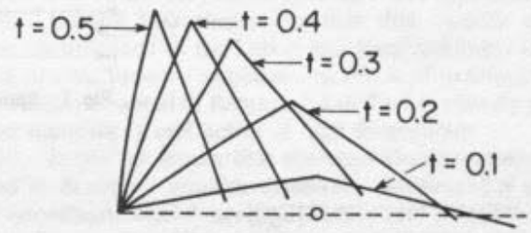

Fig. 5(*b*) Multibody dynamics: displacement driven, multi-component robot arm. Repositioning sequence to stop angle $\psi = 1.5$ rad. Time step size $h = 0.1$.

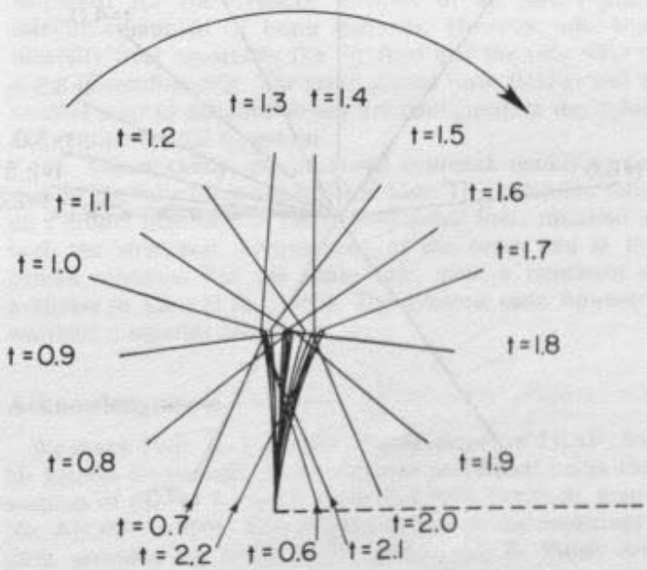

Fig. 5(c) Multibody dynamics: displacement driven of multi-component robot arm. Vibration of robot arm about stop angle, and revolution of flexible appendage about connecting hinge. Time step size $h = 0.01$, plot after each 10 time increments.

Material Properties:
$EA = GA_s = 1{,}000{,}000.$
$EI = 10{,}000.$
$A_\rho = 1.$
$I_\rho = 1.$ for link A
$I_\rho = 10.$ for link B
Fe Mesh: 4 quadratic elements.

Time history of F(t) and T(t)

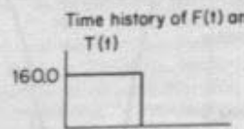

F(t) = T(t)/4.

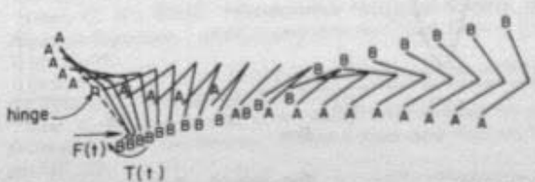

Fig. 6 Multibody dynamics: articulated beam in free flight. Time step size $h = 0.05$, plot after each 5 time increments.

Material Properties

$EA = 2.8 \times 10^7$

$GA_s = 1 \times 10^7$

$EI = 1.4 \times 10^4$

$A\rho = 1.2$

$I\rho = 6 \times 10^{-4}$

F.E. Mesh: 4 quadratic elements

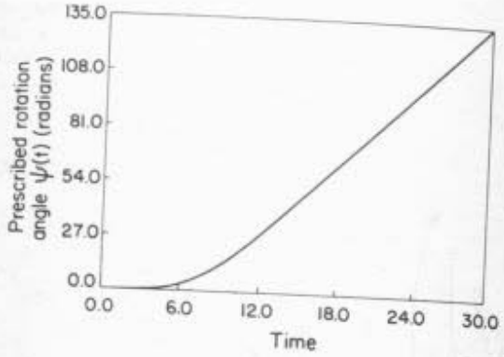

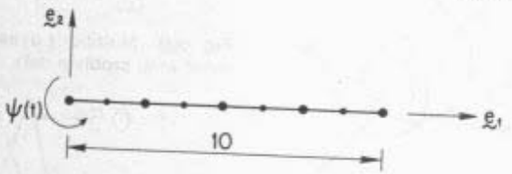

Fig. 7 Spin-up maneuver; problem data

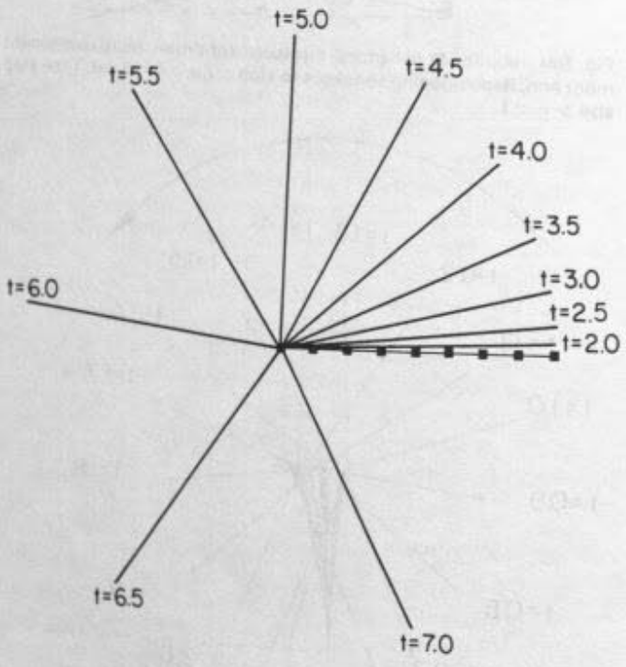

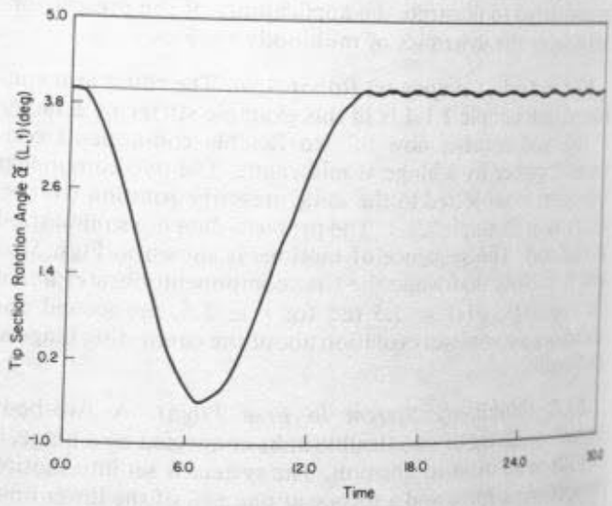

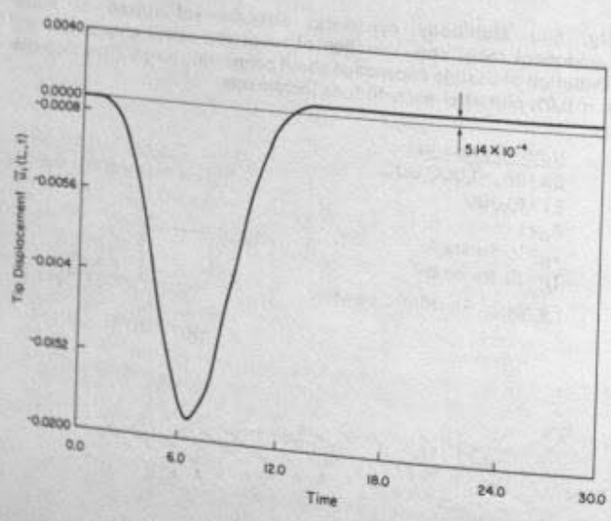

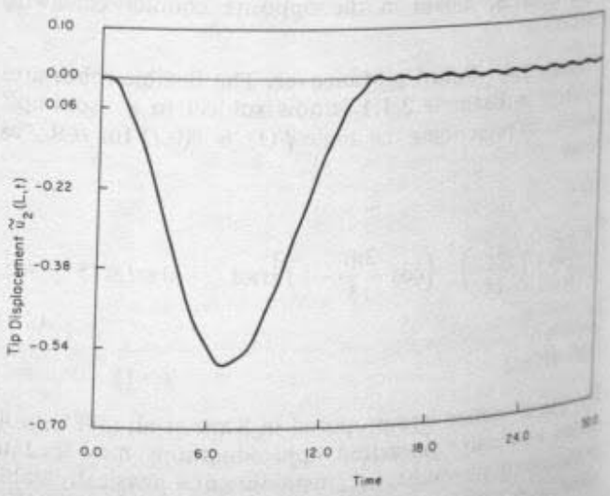

Fig. 8(a)–(d) Spin-up maneuver. Several deflected shapes during first revolution. Time histories for displacement components and section rotation relative to the shadow beam. Time step size $h = 0.005$.

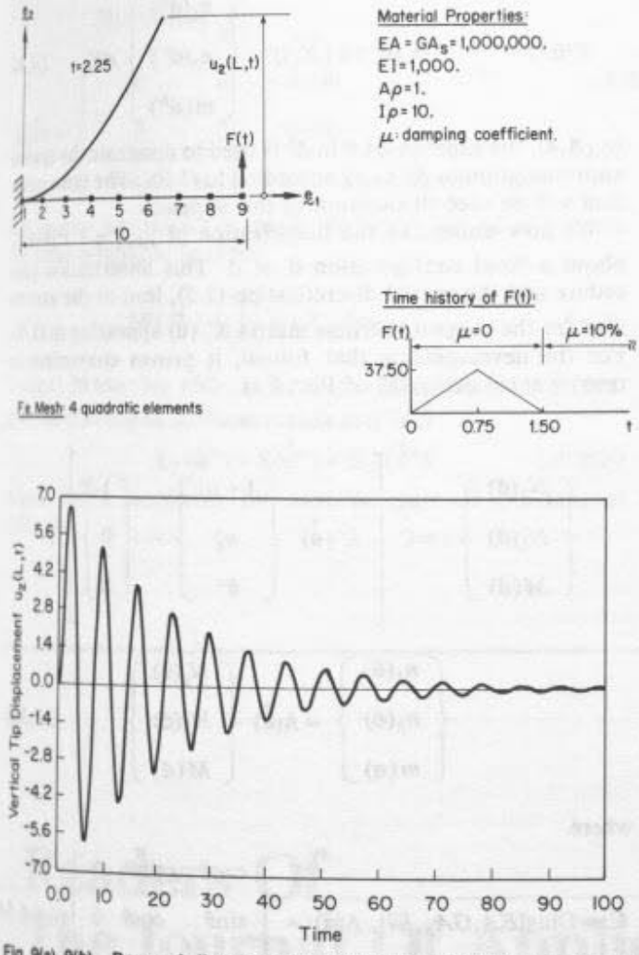

Fig. 9(a), 9(b) **Damped vibration: cantilever beam. Velocity proportional viscous force; problem data; maximum deflected shape; time history of vertical tip displacement.**

7. Deflected shapes for several values of t during the first revolution are depicted in Fig. 8. Also shown in this figure are the time histories of the displacements $\tilde{u}_1(L,t)$, $\tilde{u}_2(L,t)$ relative to the shadow beam, and the section rotation $\tilde{\alpha}(L,t)$. The results of Fig. 8 clearly exhibit the *centrifugal stiffening* effect: after an initial deflection during the acceleration phase, $t\in[0,15]$, the centrifugal force straightens the robot arm in the constant angular velocity phase, $t > 15$. The exact solution for the steady state extension of a pinned-free beam with length L, axial stiffness EA and mass per unit length ρA, spinning with constant angular velocity ω can be easily shown to be

$$\tilde{u}_1(X,t) = L\left[\frac{\tan aL}{aL} - 1\right]; \text{ where } a = \sqrt{\frac{\rho A}{EA}}\,\omega \qquad (2.2)$$

For this particular example ω = 6rad/sec, L = 10 and $\rho A/EA$ = $3/7 \times 10^{-7}$. Expression (2.2) then leads to a steady state extension at the free end of $\tilde{u}_1(L,t) = 5.14 \times 10^{-4}$. This result is in complete agreement with the computed solution (see Fig. 8). The small periodic vibration of the beam about the floating frame during this steady state phase is noted.

Example 2.5. Damped Finite Vibration of a Cantilever Beam. This example illustrates how simply viscous effect can be included in our formulation. A cantilever beam is initially subject to a concentrated end load. Subsequently, the load is removed, and the beam undergoes free vibration. Figure 9 shows the material properties, the maximum deflected shape, and the time history of the vertical tip displacement. Only *velocity* proportional damping is considered here; more general dissipative mechanisms warrant a separate treatment.

3 Concluding Remarks

We recall that in the proposed approach the inherent nonlinear character of the problem is transferred to the stiffness part of the equations of motion. This approach results in equations of motion that arise typically in nonlinear structural dynamics. Consequently, the dynamics of flexible beams under large overall motions can be analyzed in any existing nonlinear finite element program, as demonstrated through several numerical examples. Without alteration in the formulation, one can apply this approach to the dynamics of a system of flexible beams connected by hinges, as shown in examples 2.3.1 and 2.3.2. Further, we will address the following points in forthcoming publications:

(*i*) The approach proposed in this paper can be readily extended to accommodate inelastic constitutive behavior. In particular, general viscoelastic response that extends classical linear models such as the Kelvin and standard linear solids to finite strains. In many applications, this is of practical importance since, as noted in Remark 3.6 of Part I, velocity proportional damping is ineffective at high frequencies.

(*ii*) It will be shown that the algorithmic treatment proposed in Section 4 remains essentially unchanged if generalized viscoelastic models are considered. Only a modified stress update is necessary. This applies to more sophisticated models accounting for damage effects.

(*iii*) The methodology presented in this paper can be employed for the dynamic analysis of an earth-orbiting satellite composed of beam elements. However, one must carefully treat separately the far field and the near field to avoid ill-conditioning. The gravitational force field as well as satellite control actuator forces are configuration dependent and require special treatment.

iv) Conceptually, the proposed approach readily carries over to the fully three dimensional case. This extension relies on a proper treatment of three dimensional finite rotations in both the structural deformations of the beam and in the overall motions. For the static case, such a treatment is available in Kane et al. (1985). The dynamic case, however, warrants a separate treatment.

Acknowledgments

We thank Prof. R. L. Taylor, the developer of FEAP, for his helpful discussions. This work was performed under the auspices of the Air Force Office of Scientific Research, grant No. AFOSR-83-0361. This support as well as the encouragement provided by Profs. K. S. Pister and E. Polak are gratefully acknowledged.

References

Belytschko, T., and Hughes, T. J. R., 1983, *Computational Methods for Transient Analysis*, Elsevier Science Publishers.

Benson, D. J., and Hallquist, J. O., 1985, "A Simple Rigid Body Algorithm for Structural Dynamics Program. Part I," *Proc. of the Int. Conf. on Numerical Methods in Engineering Theory and Applications, Swansea*, Middleton, J., and Pande, G. N., eds., A. A. Balkema Publishers, Netherlands.

Chorin, A. J., Hughes, T. J. R., McCracken, M. F., and Marsden, J. E., 1978, "Product Formulas and Numerical Algorithms," *Communications on Pure and Applied Mathematics*, Vol. 31, pp. 205-256.

Dalhquist, G., 1963, "A Special Stability Problem for Linear Multistep Methods," *BIT*, Vol. 3, pp. 27-43.

Gear, C. W., 1971a, "Simultaneous Numerical Solution of Differential-Algebraic Equations," *IEEE Transaction on Circuit Theory*, Vol. CT-18, No. 1, pp. 89-95.

Gear, C. W., 1971b, *Numerical Initial Value Problems in Ordinary Differential Equations*, Prentice-Hall, New Jersey.

Gear, C. W., and Petzold, L. R., 1984, "ODE Methods for the Solution of Differential/Algebraic Systems," *SIAM J. Numerical Analysis*, Vol. 21, No. 4, pp. 716-728.

Goodreau, G. L., and Taylor, R. L., 1973, "Evaluation of Numerical Methods in Elastodynamics," *Comp. Meth. Appl. Mech. Engrg.*, Vol. 2, pp. 69-97.

Hilber, H. M., 1976, "Analysis and Design of Numerical Integration Methods in Structural Dynamics," Earthquake Engineering Research Center, EERC Report No. 76-29, University of California, Berkeley.

Hughes, P. C., 1979, "Dynamics of a Chain of Flexible Bodies," *The J. of the Astronautical Sciences*, Vol. 27, pp. 359-380.

Kane, T. R., Ryan, R. R., and Banerjee, A. K., 1985, "Dynamics of a Beam Attached to a Moving Base," *AAS/AIAA Astrodynamics Specialist Conference*, Paper AAS 85-390, Vail, Colorado, August 12-15.

Likins, P. W., 1974, "Dynamic Analysis of a System of Hinge Connected Rigid Bodies With Nonrigid Appendages," NASA Technical Report 32-1576.

Meirovitch, L., 1970, *Analytical Methods in Vibrations*, MacMillan, Toronto, Canada.

Newmark, N. M., 1959, "A Method of Computation for Structural Dynamics," *ASCE J. of the Engineering Mechanics Division*, pp. 67-94.

Petzold, L. R., 1982, "Differential/Algebraic Equations are not ODE's," *SIAM J. Sci. Stat. Comput.*, Vol. 3, No. 3, pp. 367-384.

Richtmyer, D., and Morton, K. W., 1967, *Difference Methods for Initial Value Problems*, Second edition, Interscience, New York, 1967.

Song, J. O., and Haug, E. J., 1980, "Dynamic Analysis of Planar Flexible Mechanism," *Comp. Meth. Appl. Mech. Engrg.*, Vol. 24, pp. 359-381.

Sunada, W., and Dubowsky, S., 1980, "The Application of Finite Element Method to the Dynamic Analysis of Flexible Spatial and Co-Planar Linkage Systems," *J. of Mechanical Design*, Vol. 103, pp. 643-651.

Zienkiewicz, O. C., 1977, *The Finite Element Method*, third edition, McGraw-Hill, New York.

APPENDIX

Finite Element Matrices

In this appendix, we shall give the expressions of the relevant matrices discussed in Section 1; namely, the mass matrix $\mathbf{M}$, the damping matrix $\mathbf{D}$, the internal forces vector $\mathbf{P}(\mathbf{d})$, the tangent stiffness matrix $\mathbf{K}_T(\mathbf{d})$, and the applied forces vector $\mathbf{F}(t)$.

Using the spatial discretization (1.3) in the first term of the weak form of the equations of motion (1.2), i.e., the inertia term, the mass matrix is obtained at once as

$$\mathbf{M}=\int_{[0,L]} \mathbf{\Psi}^t(X_1)\mathbf{I}\mathbf{\Psi}(X_1)dX_1 \tag{A.1a}$$

with

$$\mathbf{\Psi}(X_1):=[\mathbf{\Psi}_1(X_1),\ldots,\mathbf{\Psi}_N(X_1)] \tag{A.1b}$$

The damping matrix $\mathbf{D}$ is obtained exactly as in (A.1a), but with $\mathbf{\Delta}$ in the place of $\mathbf{I}$.

Next, by making use of (3.17) and (3.18) of Part I, we may rephrase the third term in the weak form (1.2) as follows

$$\boldsymbol{\eta}:=\eta_1\mathbf{e}_1+\eta_2\mathbf{e}_2+\eta_3\mathbf{e}_3,$$

$$\int_{[0,L]} \boldsymbol{\eta}\cdot\mathbf{P}[\mathbf{d}]dX_1=-\int_{[0,L]} [\eta_1 n_1'+\eta_2 n_2'+\eta_3 m' +\eta_3\{(1+u_1')n_2-u_2'n_1\}]dX_1 \tag{A.2}$$

Integrate by parts $(A.2)_2$, and recall that $\eta_1 n_1+\eta_2 n_2+\eta_3 m=0$ at the boundaries. There results

$$\int_{[0,L]} \boldsymbol{\eta}\cdot\mathbf{P}[\mathbf{d}]dX_1=\int_{[0,L]} \mathbf{D}_1(\mathbf{d})\boldsymbol{\eta}\cdot\begin{Bmatrix} n_1(\mathbf{d}) \\ n_2(\mathbf{d}) \\ m(\mathbf{d}) \end{Bmatrix} dX_1 \tag{A.3a}$$

with $\mathbf{D}_1(\mathbf{d})$ denoting the following differential operator

$$\mathbf{D}_1(\mathbf{d}):=\begin{bmatrix} \dfrac{d}{dX_1} & 0 & u_2' \\ 0 & \dfrac{d}{dX_1} & -(1+u_1') \\ 0 & 0 & \dfrac{d}{dX_1} \end{bmatrix} \tag{A.3b}$$

Introducing the discretization $(1.3)_2$ into $(A.3a)$, we obtain the expression for the discrete internal forces

$$\mathbf{P}(\mathbf{d}^h)=\int_{[0,L]} [\mathbf{D}_1(\mathbf{d}^h)\mathbf{\Psi}(X_1)]^t \begin{Bmatrix} n_1(\mathbf{d}^h) \\ n_2(\mathbf{d}^h) \\ m(\mathbf{d}^h) \end{Bmatrix} dX_1 \tag{A.4}$$

In (A.4), the superscript h in $\mathbf{d}^h$ is used to designate the spatial approximation to $\mathbf{d}(X_1,t)$ according to $(1.3)_1$. The same notation will be used throughout in this appendix.

We now undertake the linearization of $\int_{[0,L]} \boldsymbol{\eta}\cdot\mathbf{P}[\mathbf{d}]dX_1$ about a fixed configuration $\mathbf{d}\equiv\mathring{\mathbf{d}}$. This linearization procedure and the spatial discretization (1.3), lead to the expression for the tangent stiffness matrix $\mathbf{K}_T(\mathring{\mathbf{d}})$ appearing in (1.9). For the developments that follow, it proves convenient to rewrite equation (3.18) of Part I as

$$\begin{Bmatrix} N_1(\mathbf{d}) \\ N_2(\mathbf{d}) \\ M(\mathbf{d}) \end{Bmatrix} :=\mathbf{C}\left[\mathbf{\Lambda}^t(\mathring{\mathbf{d}})\begin{Bmatrix} 1+u_1' \\ u_2' \\ \theta' \end{Bmatrix}-\begin{Bmatrix} 1 \\ 0 \\ 0 \end{Bmatrix}\right],$$

$$\begin{Bmatrix} n_1(\mathbf{d}) \\ n_2(\mathbf{d}) \\ m(\mathbf{q}) \end{Bmatrix} =\mathbf{\Lambda}(\mathring{\mathbf{d}})\begin{Bmatrix} N_1(\mathbf{d}) \\ N_2(\mathbf{d}) \\ M(\mathbf{d}) \end{Bmatrix} \tag{A.5a}$$

where

$$\mathbf{C}:=\mathrm{Diag}[EA,GA_S,EI],\ \mathbf{\Lambda}(\mathring{\mathbf{d}}):=\begin{bmatrix} \cos\theta & -\sin\theta & 0 \\ \sin\theta & \cos\theta & 0 \\ 0 & 0 & 1 \end{bmatrix} \tag{A.5b}$$

The linearization about $\mathring{\mathbf{d}}$ is based on the notion of directional derivative at $\mathring{\mathbf{d}}$ in the direction $\Delta\mathbf{d}:=[\Delta u_1,\ \Delta u_2,\ \Delta\theta]^t$. The following linearized quantities are needed:

$$\frac{d}{d\epsilon}\bigg|_{\epsilon=0}\mathbf{\Lambda}\ [\mathring{\mathbf{d}}+\epsilon\Delta\mathbf{d}]=\begin{bmatrix} 0 & -\Delta\theta & 0 \\ \Delta\theta & 0 & 0 \\ 0 & 0 & 0 \end{bmatrix}\mathbf{\Lambda}(\mathring{\mathbf{d}}), \tag{A.6a}$$

$$\frac{d}{d\epsilon}\bigg|_{\epsilon=0}\begin{Bmatrix} N_1 \\ N_2 \\ M \end{Bmatrix}(\mathring{\mathbf{d}}+\epsilon\Delta\mathbf{d})=\mathbf{C}\mathbf{\Lambda}(\mathring{\mathbf{d}})\mathbf{D}_1(\mathring{\mathbf{d}})\Delta\mathbf{d}, \tag{A.6b}$$

$$\frac{d}{d\epsilon}\bigg|_{\epsilon=0}\mathbf{D}_1(\mathring{\mathbf{d}}+\epsilon\Delta\mathbf{d})\boldsymbol{\eta}=\begin{bmatrix} 0 & 0 & \Delta u_2' \\ 0 & 0 & -\Delta u_1' \\ 0 & 0 & 0 \end{bmatrix}\boldsymbol{\eta}. \tag{A.6c}$$

The linearization of the second term in the weak form (1.2) then follows at once

$$\frac{d}{d\epsilon}\bigg|_{\epsilon=0}\left\{\int_{[0,L]} \boldsymbol{\eta}\cdot\mathbf{P}[\mathring{\mathbf{d}}+\epsilon\Delta\mathbf{d}]dX_1\right\}=$$

$$\int_{[0,L]} \mathbf{D}_1(\mathring{\mathbf{d}})\boldsymbol{\eta}\cdot\mathbf{\Lambda}(\mathring{\mathbf{d}})\mathbf{C}\mathbf{\Lambda}^t(\mathring{\mathbf{d}})\mathbf{D}_1(\mathring{\mathbf{d}})\Delta\mathbf{d}dX_1 \tag{A.7}$$

$$+\int_{[0,L]} \mathbf{D}_2\boldsymbol{\eta}\cdot\mathbf{G}(\mathring{\mathbf{d}})\mathbf{D}_2\Delta\mathbf{d}dX_1$$

in which the differential operator $\mathbf{D}_2$ and the matrix $\mathbf{G}(\mathring{\mathbf{d}})$ are defined below

$$\mathbf{D}_2 := \mathrm{Diag}\left[\frac{d}{dX_1}, \frac{d}{dX_1}, 1\right],$$

$$\mathbf{G}(\overset{*}{\mathbf{d}}) := \begin{bmatrix} 0 & 0 & -n_2(\overset{*}{\mathbf{d}}) \\ 0 & 0 & n_1(\overset{*}{\mathbf{d}}) \\ -n_2(\overset{*}{\mathbf{d}}) & n_1(\overset{*}{\mathbf{d}}) & -[(1+\overset{*}{u}_1')n_1(\overset{*}{\mathbf{d}}) + \overset{*}{u}_2' n_2(\overset{*}{\mathbf{d}})] \end{bmatrix} \quad (A.8)$$

Let us now introduce the spatial discretization of $\Delta\mathbf{d}(X_1)$ in the same manner as in $(1.3)_1$

$$\Delta\mathbf{d}(X_1) \cong \sum_{I=1}^{N} \mathbf{\Psi}(X_1)\Delta\mathbf{q}_I \quad (A.9)$$

Using (1.3) together with $(A.9)$, we finally arrive at the expression for the tangent stiffness matrix at $\overset{*}{\mathbf{d}}^h \cong \overset{*}{\mathbf{d}}$

$$\mathbf{K}_T(\overset{*}{\mathbf{d}}^h) = \mathbf{K}(\overset{*}{\mathbf{d}}^h) + \mathbf{K}_G(\overset{*}{\mathbf{d}}^h) \quad (A.10a)$$

where $\mathbf{K}(\overset{*}{\mathbf{d}}^h)$ represents the *material* part of the tangent stiffness,

$$\mathbf{K}(\overset{*}{\mathbf{d}}^h) := \int_{[0,L]} [\mathbf{D}_1(\overset{*}{\mathbf{d}}^h)\mathbf{\Psi}(X_1)]^t \mathbf{\Lambda}(\overset{*}{\mathbf{d}}^h)\mathbf{C}\mathbf{\Lambda}^t(\overset{*}{\mathbf{d}}^h)\mathbf{D}_1(\overset{*}{\mathbf{d}}^h)\mathbf{\Psi}(X_1)dX_1 \quad (A.10b)$$

and $\mathbf{K}_G(\overset{*}{\mathbf{d}}^h)$ the *geometric* part,

$$\mathbf{K}_G(\overset{*}{\mathbf{d}}^h) := \int_{[0,L]} [\mathbf{D}_2\mathbf{\Psi}(X_1)]^t \mathbf{G}(\overset{*}{\mathbf{d}}^h)\mathbf{D}_2\mathbf{\Psi}(X_1)dX_1 \quad (A.10c)$$

It is clear that the applied load vector $\mathbf{F}(t)$ is given by

$$\mathbf{F}(t) = \int_{[0,L]} \mathbf{\Psi}^t(X_1) \begin{Bmatrix} \tilde{n}_1(X_1,t) \\ \tilde{n}_2(X_1,t) \\ \tilde{m}(X_1,t) \end{Bmatrix} dX_1 \quad (A.11)$$

The integration in all of the above matrices may be performed numerically using Gauss quadrature. For the tangent stiffness matrix $\mathbf{K}_T$, we use uniform reduced integration to avoid shear locking.